ELSEVIER

Physica D 77 (1994) 238–260

PHYSICA D

Computer simulations of self-organized wind ripple patterns

Walter Landry[a,1], B.T. Werner[b,*]

[a] *Division of Physics, Mathematics and Astronomy 200-36, California Institute of Technology, Pasadena, CA 91125, USA*
[b] *Institute of Geophysics and Planetary Physics 0225, Scripps Institution on Oceanography, University of California, San Diego, La Jolla, CA 92093-0225, USA*

Abstract

A variety of surficial patterns including beach cusps, sand dunes, wind ripples, stone stripes and sorted circles have been reproduced successfully with computer simulations in which the patterns develop via self-organization and both transporting agents and transported material are discretized. As an example, three-dimensional, grain-level computer simulations of wind ripple formation are described. The results of these simulations demonstrate that a model that includes only incremental transport of surface grains by impacts from wind-propelled hopping (saltating) grains is sufficient to produce self-organized wind ripples whose size, cross-sectional shape, plan-view geometry and time evolution from an original flat surface fall within observed ranges for natural ripples. Simulated wind ripples are initiated from a flat sand bed because of an instability deriving from a dependence of transport rate on slope. A characteristic ripple spacing that is proportional to the grain diameter and increases slowly with time develops as a result of interactions and mergers between ripples. Imperfections to the ripple pattern play a significant role in the determination and evolution of the spacing of simulated ripples.

1. Introduction

Loose material on the Earth's surface such as sand, gravel and stones often is organized into patterns characterized by a definite spatial scale. These surficial patterns can be defined by relief, grain size or grain type. The grains comprising the patterns are acted upon by wind, water, gravity, ice, flora or fauna. Typical patterns include ripples and dunes in sand, beach cups and sand bars, and patterns in frozen soil such as sorted circles and stone stripes. Despite much research on these patterns, the nature of the connection between the processes causing grain rearrangement and the patterns that develop remains controversial.

An understanding of the relationship between environment, processes and surficial patterns is a long-standing goal of geology and geomorphology. For example, the dependence of dune form and deposits on wind speed and direction can be used to infer past climatic conditions from the morphology and stratigraphy of an active sand dune field (reviewed, e.g., in [1]). On a more fundamental level, study of particular natural systems can illuminate the role and character of feedbacks in the formation of patterns. Fundamental issues include (i) understanding how

* To whom correspondence should be addressed.
[1] Present address: Department of Astronomy, 516 Space Science, Cornell University, Ithaca, NY 14853, USA.

SSDI 0167-2789(94)00122-7

simple surficial patterns emerge from complicated transport mechanisms, (ii) determining the general processes that influence the spatial scale of the patterns, and (iii) identifying the properties shared by similar patterns that form in diverse systems.

One technique for addressing these issues is the use of computer simulations in a manner similar to laboratory experimentation. Model systems are created that isolate particular aspects of the pattern under study and various measurements are made under controlled conditions to determine those underlying physical behaviors that can account for the observed macroscopic pattern. This is an inverse problem, with the pattern being specified and the solution being the class of underlying "rules" or microscopic physical laws that generate the pattern. In this paper, and in other related work, this inverse problem is constrained by the requirement that the "rules" determining the behavior of the simulated system at the microscopic level correspond closely to physical processes known to be operating in the system at hand.

One technique for simulating surficial patterns, adopted in this paper, is to retain the explicitly discrete character of the sand, stones or soil comprising the pattern. In contrast, in a more traditional approach, the surface elevation, the transport rate and other surface properties are treated as continuous variables related by differential equations, which are discretized only for numerical solution (e.g., [2]). However, continuum models may not capture essential features of patterns [3]. Moreover, in some cases, it is advantageous to model a nominally continuous transporting agent, such as a flowing fluid, with (discrete) particles [4,5]. Particle techniques for modeling the transport of sediment facilitate mixed Lagrangian and Eulerian descriptions of the coupled fluid-sediment system and treatment of problems involving complicated or moving boundaries [6,7].

Transverse bedforms develop where sand or gravel is transported in a narrow range of directions. Transverse bedforms are composed of a series of roughly evenly spaced alternating ridges and troughs oriented perpendicular to the sediment transport direction. Examples include ripples on desert dunes, in rivers and in the reversing currents under waves, sand dunes resulting from wind and water flow, and sand bars that form close to the shores of lakes and oceans. Transverse bedforms commonly are characterized by a narrow distribution of spacings between ridge crests.

Langbein and Leopold [8] likened transverse bedforms to kinematic waves, where a maximum in the transport flux as a function of surface grain concentration or elevation causes a flat surface to be unstable. To investigate the fundamental principles underlying the formation of bedform patterns, we consider a particularly striking example of a transverse bedform: wind ripples (Fig. 1). Wind ripples are gentle undulations of a surface composed of loose sand grains, oriented roughly perpendicular to the wind direction and with a mean spacing between ripple crests, λ, corresponding to the peak of the spacing distribution [9]. The mean spacing is approximately proportional to the mean grain diameter, d; for dune sand, $d \sim 0.025$ cm. Typical values for λ fall in the range $200d$ to $300d$ [10]. The difference in elevation between crest and trough, the ripple height h, is about $15d$ on mature ripples, and the ripple index, $i = \lambda / h$, commonly lies between 15 and 20 [10]. The crests of well-formed wind ripples are continuous over a length that is much greater than their mean spacing [11]. Wind ripples develop and propagate downwind by transport of surface grains through the indirect action of the wind, as explained in more detail below. The morphology of wind ripples is similar to many other transverse bedforms, suggesting that an understanding of their fundamental dynamics could have wide application.

In this paper we will present a new three-dimensional computer simulation model of wind ripple formation, and focus on simulation tests that bear on the manner in which ripples arise

Fig. 1. Oblique view of wind ripples at the Algodones Dunes, California. Wind is from the bottom and ripple spacing is approximately 10 cm.

from a flat surface and on the origin of a characteristic spacing.

2. Background discussion of wind ripples

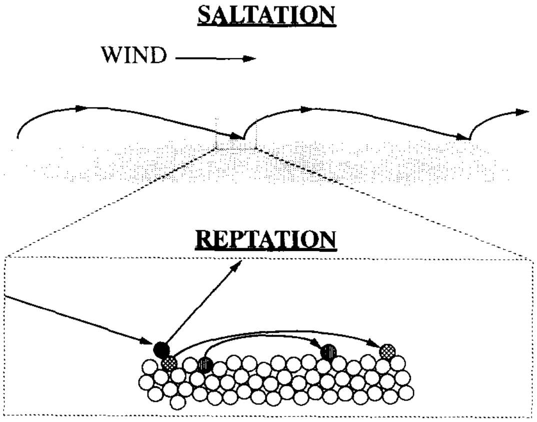

Fig. 2. Dune sand is transported by the wind in two modes. Grains in *saltation* are accelerated by the wind on long, low-angle hopping trajectories. The impact of saltating grains with the bed ejects surface grains on short quasi-ballistic trajectories (with little modification by the wind). This second transport mode, *reptation*, is hypothesized to be responsible for the rearrangement of grains on the bed into wind ripples. The exchange flux between saltating and reptating grain populations is believed to be small [12,13,15].

Wind ripples form through a rearrangement of sand grains on a sand bed into ridge crests and troughs. This rearrangement is believed to take place by a mechanism in which the wind plays only an indirect role. In *saltation*, grains hop along the surface, propelled by the wind on long, low-angle trajectories [9], Fig. 2. According to theory [12], computer simulations [13,14] and experiments [9,15], most saltating grains rebound from the surface upon impact and continue in saltation. Impacts between saltating grains and the bed eject surface grains into saltation to replace those that come to a stop [16]. These impacts also eject a number of grains on short, quasi-ballistic trajectories that are largely unaffected by the wind. This secondary population of transported grains, driven by the saltating grains, is said to be in *reptation* (also termed surface creep) [9,17], Fig. 2. Saltating grains travel with a wide distribution of velocities and hop lengths, implying a lack of spatial correlation between successive hops. The impact angle relative to the horizontal for saltating grains with sufficient energy to eject surface grains into reptation is narrowly distributed in the range 10°–15° [9]. It has been argued theoretically [12] that surface grains will not be ejected from a flat surface by direct aerodynamical forces if sand is being transported in steady-state saltation; it is not known whether this conclusion is modified by the presence of wind ripples. As wind velocity is increased, the impact velocity and impact angle of the fastest moving saltating grains increases.

In summary, the rearrangement of grains into ripples is assumed to be accomplished primarily through the random impacts of saltating grains with the grain bed. Experiments [18] and computer simulations [19] indicate that the mean total downwind distance grains are moved per saltating grain-bed impact, l_r – the reptation length, varies in the range 50–150d and is shared among 2–6 primary grains.

Without attempting an extensive review of past models and observations of ripple formation (see, e.g., [20]), some of the models and observations directly relevant to the simulations described in this paper will be discussed briefly. In his classic monograph on wind-blown sand, Bagnold [9] advanced the theory that the spacing of ripples corresponds to an average hop length for saltating grains. He reasoned that the change in the impact flux on the upwind side of a ripple caused by the variation of the slope there would be reflected in the impact flux one average saltating grain hop length downwind. Assuming that transport in reptation is proportional to the impact flux, he concluded that for ripples to be steady-state propagating forms, the surfaces separated by one hop length would have to evolve to the same slope, thereby fixing the ripple spacing equal to one hop length. Subsequent theory and measurements have found that hop lengths for saltating grains have a wide distribution [21–22]. Moreover, in a computer simulation of ripple formation using a fixed saltation hop length, the effect of variation of impact flux with surface slope was overwhelmed by other factors [23]. The results of a recent computer model [24] support a near equality of saltating grain hop length and ripple spacing. It is not clear that this recent model incorporates the critical elements of sand transport on ripples by the wind, namely a dominance of erosion and deposition by impact-induced reptation.

In a model applied to ripples and dunes formed in air and underwater, Kennedy [25] proposed that sinusoidal perturbations to the interface between the grain surface and the fluid develop into finite amplitude bedforms. The spacing of the fastest growing bedform is determined by a lag distance between surface slope and surface grain transport rate. For wind ripples, Kennedy used a very general relationship between sand flux and wind velocity and did not treat the details of wind-blown sand transport. Anderson [26] reformulated the Kennedy model in terms of a population of reptating grains driven by a uniform flux of saltating grain-bed impacts and concluded that $\lambda \sim 4$–$6l_r$. One assumption of these models, noted by both Kennedy and Anderson, is that the sand surface elevation is linear in the presence of small-amplitude ripples. In this context, linear refers to an absence of interactions between ripples of different amplitudes and spacings, implying superposition. This assumption contradicts field observations and computer simulations of wind ripples, where small ripples frequently undergo nonlinear mergers [3,10,18,20]. Both the perturbation models and the Bagnold characteristic hop length model fail to explain the progressive increase of wind ripple spacing observed in the field and in wind tunnels.

A levelled sand surface over which grains are saltating develops a mottled appearance that within minutes is transformed into an imperfectly connected series of sand ridges oriented perpendicular to the wind direction [10]. With time, the mean spacing between ripple crests increases at a decreasing rate until an apparently stable mean spacing is attained. The pattern evolves toward ripples with long, continuous crests and a low density of imperfections to the pattern (ripples crests that terminate) in at time that may vary from 10–30 minutes, depending on conditions [10,27]. Shortly after initiation, ripples with a distribution of sizes are observed. Ripples then interact because small ripples propagate faster than large ripples. (This may be understood as a surface-to-volume effect: transport occurs only on the surface but the entire volume of the ripple must be moved downwind for propagation.) Viewed in cross section, these interactions sometimes result in mergers (Fig. 3a), or alternatively in an exchange of sand between smaller and larger ripples, repulsion (Fig. 3b). In a field of ripples covering the surface, mergers are the only means for increasing the mean ripple spacing. The observed decreasing rate of ripple growth with increasing size implies that mergers are the dominant interaction at small ripple spacings, and repulsion is dominant at larger spacings.

The development of wind ripples described above has been observed in two-dimensional (cross-sectional) computer simulations of sand grain transport in reptation by random impacts of saltating particles [18,20,23,28]. The simulation results have prompted the hypothesis that wind ripples are self-organized, i.e., that the long-range order characterizing the ripple pattern results from spatially local interactions among saltating, reptating and surface grains. Although simulated ripples can be made to be remarkably similar in spacing, shape and time evolution to natural ripples, questions still remain regarding the correspondence between natural and simulated ripples and regarding the physics of how ripples initiate and evolve in the computer simulations. A recent theoretical model for wind ripples that addresses the problem of ripple spacing evolution with time (3) is discussed in Section 4.6.

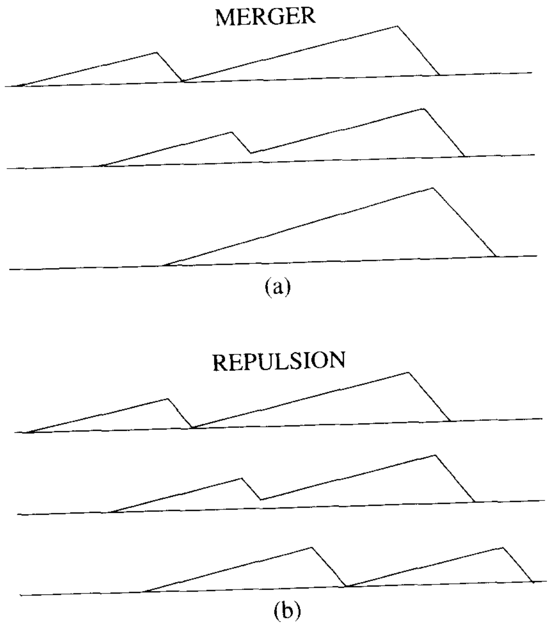

Fig. 3. Idealized cross-sectional views of wind ripple interactions observed in the field and in computer simulations. Ripples with a distribution of sizes interact because propagation speed is inversely proportional to size. Wind is from left to right. (a) A sequence showing a small ripple climbing the upwind face of a larger ripple and merging with it. (b) A small ripple climbs the upwind face of a larger ripple, capturing some of the larger ripple's sand. The result is an exchange in the ordering of sizes, and hence an effective repulsion of the two ripples. A merger tends to occur when the scale of both ripples is small; repulsion is more common where the scale of both ripples is large.

3. Wind ripple algorithm

In this section, an algorithm is described that is designed to investigate the consequences in three dimensions of the hypothesis that wind ripples form and evolve entirely through the transport of grains in reptation driven by randomly located saltating grain-bed impacts. The algorithm does not treat the dynamics of the grain-bed impact; rather, the effect of the impact has been parametrized in the form of a rule specifying the number of grains ejected and the distance travelled from the impact point. To elucidate the physics of ripple formation, the grain-bed impact has been simplified. For each impact, only one surface grain is ejected. (Results of simulations in two dimensions lead to qualitatively similar results for both simple and complicated ejection patterns [23]. Additionally, the bed grains are taken to be a single size and are constrained to lie on a hexagonally close packed lattice, Fig. 4. The bed is tilted 90° from the usual orientation so that the maximum angle that grains can be stacked (in the downwind and cross wind directions), the angle of repose, is 30°, slightly less than typical values for natural sand [30]. The ends of the simulated sand bed are connected by periodic boundary conditions in both the downwind and cross-wind directions.

A simulation consists of repeatedly propelling spherical "saltating" grains on straight, low-angle trajectories in a single direction (the "wind" direction) from randomly chosen positions above the sand bed. For the results described here, the diameters of the saltating grains and the bed grains are taken to be equal. In the simplest form of the algorithm, which we term the "target" algorithm, the surface grain with which the saltating grain collides, the target grain, is transported a specified number of grain diameters l_r downwind and is lowered to the surface; then the target grain is moved down the steepest surface gradient until a stable pocket (supported by four bed grains) is found, whereupon it is deposited (Fig. 4). The movement of a deposited target grain down an angle of repose slope that is inclined to the wind direction provides the only cross-wind communication of surface elevations and gradients in the target algorithm.

Three modifications to this basic algorithm will be considered here. All three involve physics that are known to occur in reptation; however, the strength of each of these effects in determining the trajectories of reptating grains is unknown. First, in the "gradient" algorithm, the probability that the target grain is ejected from the bed and the direction that the grain is transported depend on the mean surface gradient surrounding the impact point. This is motivated by dynamical computer simulations of saltating grain-bed impacts (using an algorithm described in [13]), that show a decreasing mean reptation length as the surface is tilted upwind, Fig. 5. The direction toward which the reptated grain is deflected corresponds to the direction (projected onto a horizontal plane) of the momentum transfer in a collision between the impacting

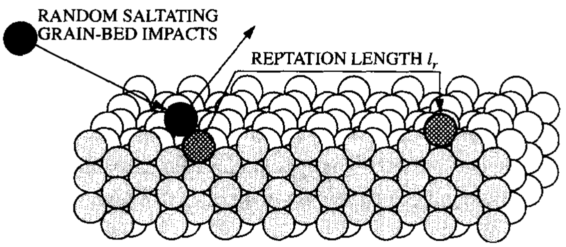

Fig. 4. Wind ripple simulation algorithm. A saltating grain originating at a random location above the bed strikes a surface grain, which is moved a distance l_r downwind and then is dropped to the surface, where it travels down the steepest gradient to a stable lattice site (the target algorithm). The saltating grain then is discarded.

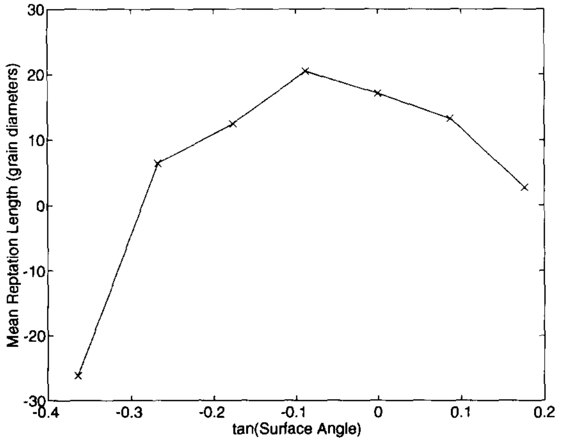

Fig. 5. Mean reptation length (per impact) vs. tangent of the angle of incline of the surface for saltating grains approaching the surface at 10° relative to the horizontal. From a dynamical computer simulation, averaged over 200 impacts.

particle and a flat plane fit to the positions of the 48 surface grains surrounding the target grain.

We note that the trend observed in dynamical grain-bed impact simulations that reptation length *decreases* with increasing upwind tilt conflicts with calculations inferred from wind-tunnel observations of grain-bed impacts on sloping surfaces [31], where the reptation flux was found to *increase* with increasing upwind tilt. Questions exist regarding the applicability of these wind tunnel results because of possible time-dependent sorting effects due to the use of a range of grain sizes, the failure to observe the bed directly and the contradiction of the wind tunnel data with the necessity that reptation flux is at a maximum at the crest of the ripple (by mass conservation and the observation that natural ripple profiles are nearly flat in the vicinity of the crest: [32]).

The second modification to the target algorithm, the "straight ahead" algorithm, applies the gradient algorithm with the constraint that the target grain is transported in reptation directly downwind irrespective of surface gradient. The third modification, the "rolling" algorithm, employs the gradient algorithm and assigns the target grain a quantity we term pseudo-momentum, which permits the grain to travel beyond the first stable pocket it encounters. For the simulations discussed in this paper, a target grain is given 5 units of pseudo-momentum when it is dropped to the sand bed. Each time the grain moves one grain diameter upslope, it loses 2 units of pseudo-momentum, each time it moves downslope it gains 1 unit of pseudo-momentum, and each time it moves one lattice spacing without gaining or losing elevation, it loses 1 unit of pseudo-momentum. A number of other modifications to the target algorithm, including sensitivity to local relief and dynamical interference between nearby impacts, have been discussed elsewhere for two-dimensional wind ripple simulations [23].

The spacing, height, and ripple index are measured by searching along the bed in the downwind direction for successive significant local maxima (crests) and minima (troughs) in the surface elevation. A ripple is defined as ranging from the lowest point of one trough to the lowest point of the next trough downwind. The height of a ripple then is the average of the elevation differences going from the first trough to the crest and from the crest to the second trough. The spacing between two ripples is calculated as the average of the trough-to-trough distance and the distance from the crest of the ripple to the next ripple crest downwind. The ripple index is the ratio of spacing to height calculated for each ripple. These values are averaged in the cross wind direction to obtain the spacing, height and index distributions, from which mean values and standard deviations are calculated.

In the simulations, time t is measured in units of the mean number of saltating grain-bed impacts per exposed surface grain on a flat surface. For a typical sand flux, one unit in t may correspond to a time of about 1 s [23,33]. Distances are measured in terms of the grain diameter. The reptation length (measured in grain diameters) and the size of the periodic lattice also can influence the spatial scale of simulated wind ripples.

4. Results

4.1. General picture

The general development of simulated wind ripples from a flat surface bears a close resemblance to the formation sequence described above for natural ripples. Using the gradient algorithm on a lattice with horizontal size 1024×1024 (for $d = 0.025$ cm, ~25 cm × 21 cm), impact angle to the horizontal 10°, and a maximum reptation length $15d$, the bed initially assumes a mottled appearance, shown in Fig. 6a at $t = 20$, and is characterized by roughly coherent, organized sand piles approximately 2–$3d$ in height. At

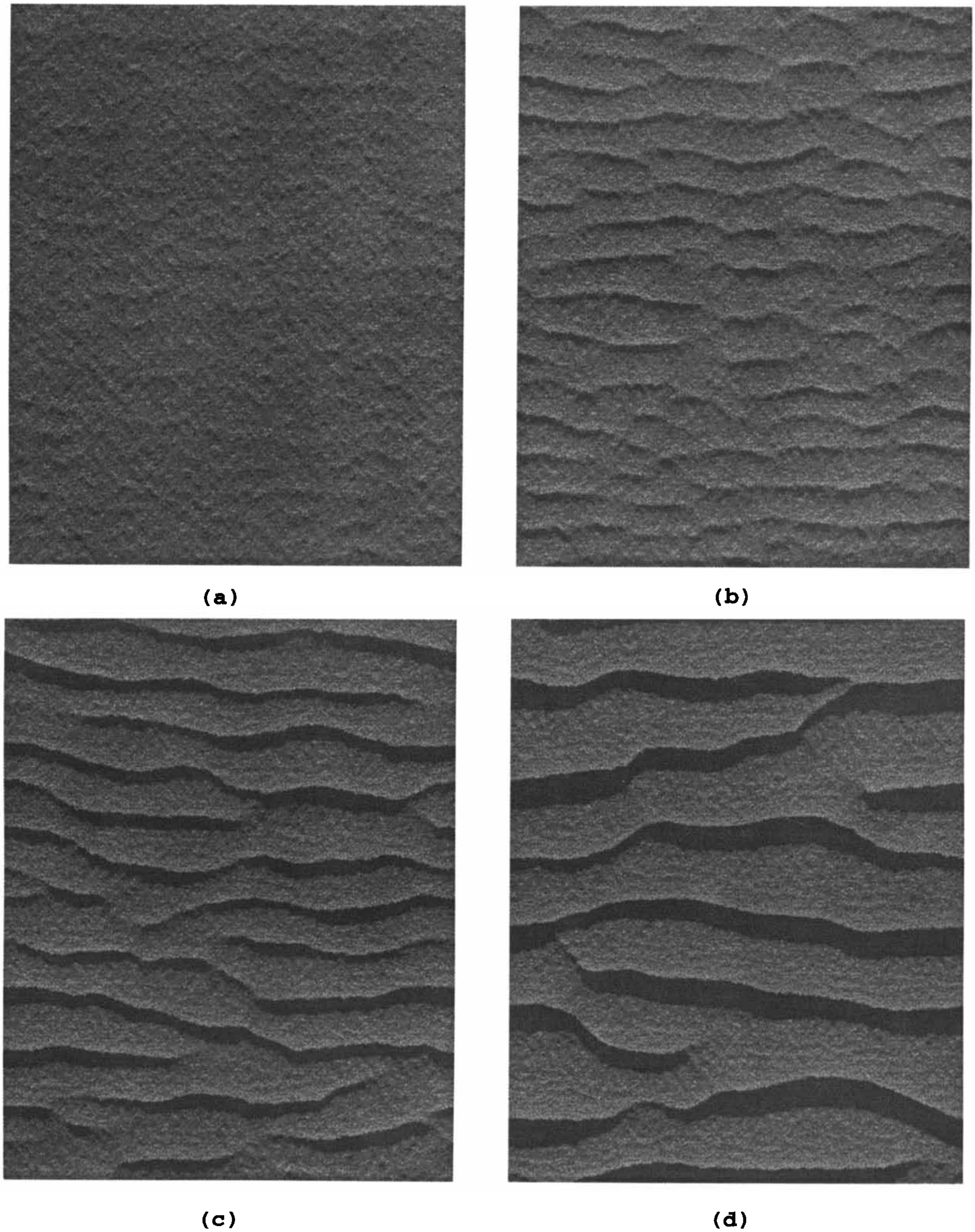

Fig. 6. Plan view of the development of computer simulated wind ripples using the gradient algorithm. "Wind" (≡impacting particles) is from the bottom in this and all other plan views. Lighted from the bottom with angle 11° relative to the horizontal. Dark areas are shadows on the downwind side of the ripple. 1024×1024 periodic lattice, with top-to-bottom length $= 1024d$, width $= 836d$. (a) $t = 20$. (b) $t = 60$. (c) $t = 200$. (d) $t = 500$.

$t = 60$ (Fig. 6b), sand ridges that are fairly continuous transverse to the "wind" direction (i.e., the direction of motion of the impacting grains) and that have an associated mean spacing of about $60d$ have developed. Figs. 6c–d document the increasing spacing and transverse connectivity of the ripple pattern with time (at $t =$ 200 and 500 respectively). The mean spacing increases by mergers between ripples in a manner described in detail below. The ripples propagate in the direction of the wind. For example, at $t = 200$ and $\lambda = 150d$, the mean ripple propagation speed is approximately $0.8d$/impact, corresponding to propagating one ripple spacing in about 3 min., or a speed of 1.2 cm/min. for $d = 0.025$ cm and a typical saltation flux. This value is close to the ripple propagation speed measured on dunes at the lowest wind velocity required to initiate sand motion, ~1 cm/min. (10).

The general picture outline above and the approximate mean quantities measured in the simulations do not appear to be sensitive to sand bed size (varying from 256×256 to 1024×1024) when the system contains at least about 5 ripples (except for the uncertainty in ripple size due to the finite fetch). Longer simulations with larger systems will allow the influence of system size to be addressed more quantitatively.

4.2. Transport algorithm

To assess the sensitivity of the ripple pattern to the transport algorithm employed, ripples resulting from the four algorithms discussed above and the target and gradient algorithms restricted to two dimensions are compared in this section. A plan view of simulated ripple patterns at $t = 300$ is shown in Fig. 7 and the corresponding ripple cross sections are displayed in Fig. 8. Steep ripples with upwind slopes of 20°–25°, downwind slopes at the angle of repose, 30°, and intervening flat zones are produced by the target algorithm. Ripples characterized by gentler upwind slopes varying from about 8° to 14° result from application of the gradient and straight ahead algorithms. Ripples generated by the rolling algorithm form a well-defined and regular pattern, despite their very gentle upwind and downwind slopes. An increase in the "strength" of the gradient or rolling aspects of the algorithm beyond the parameters used in the rolling simulation inhibits ripple formation entirely. (For the gradient algorithm, increasing the "strength" implies increasing the sensitivity of reptation length to surface gradient; for the rolling algorithm, increasing the "strength" implies permitting the target grain to travel longer distances after being dropped to the surface, either by increasing the initial pseudo-momentum or by decreasing the loss of pseudo-momentum when moving upslope). The straight ahead, gradient and rolling algorithms generate ripples with asymmetrical cross-sectional profiles as are found in nature (Fig. 8). Both target and straight ahead algorithms, characterized by only weak communication in the cross-wind direction, generate ripples with sinuous crests. By contrast, the gradient and rolling algorithms yield ripple patterns with nearly straight crests.

Mean ripple spacing and height as a function of time are plotted in Figs. 9, 10 for the target, straight ahead and gradient algorithms. In all cases, the mean spacing and height increase monotonically with time. Gentler upwind slopes result in slower growth rates. A fairly close correspondence between two and three dimensions is observed. The mean simulated ripple spacing varies from $100d$ to $200d$ at $t = 400$ (~7 min), the mean height from $7d$ to $25d$, and the mean ripple index from 8 to 15. (A larger index, on the order of 30–40, was observed for the rolling algorithm, but it was not measured accurately by the automatic crest and trough finding routine because of the small magnitude of the height.) These compare with typical ranges in the field for mature ripples varying from $200d$ to $350d$ for spacing, $10d$ to $20d$ for height and 15 to 20 for index [10]. The mean spacing and height for simulated ripples are

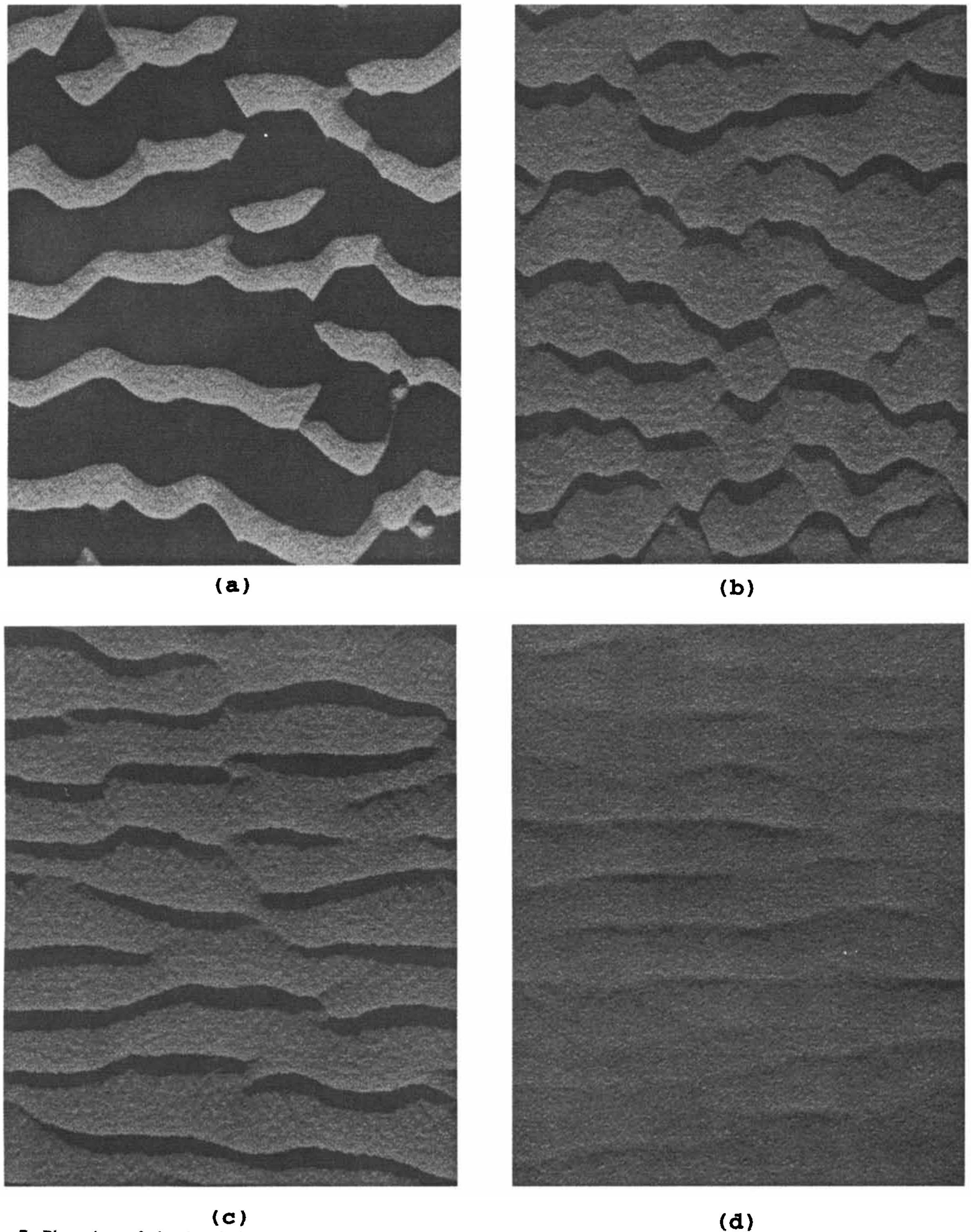

Fig. 7. Plan view of simulated ripples at $t = 300$ for 4 different algorithms. Surface size and lighting as in Fig. 6. (a) Target algorithm. (b) Straight ahead algorithm. (c) Gradient algorithm. (d) Rolling algorithm. Note the progression to straighter crests and smaller ripple index here and in Fig. 8.

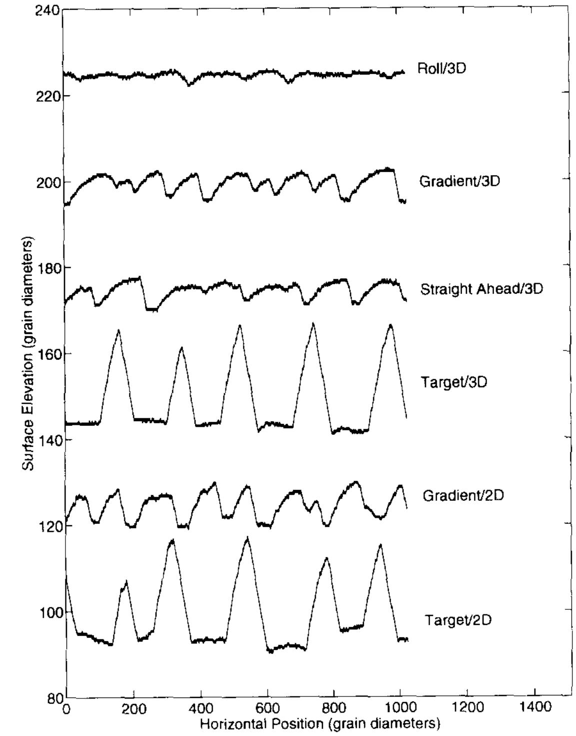

Fig. 8. Cross-sectional view of simulated ripples at $t = 300$ for 7 different algorithms in two and three dimensions. Impacting particles move from left to right. Vertical coordinate exaggerated by a factor of 8.

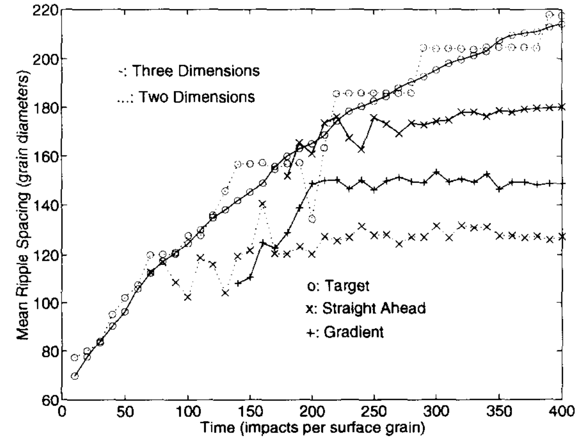

Fig. 9. Mean ripple spacing vs. time for the target, straight ahead and gradient algorithms in two and three dimensions. Ripples with a smaller index initiate at larger spacing and grow at a slower rate.

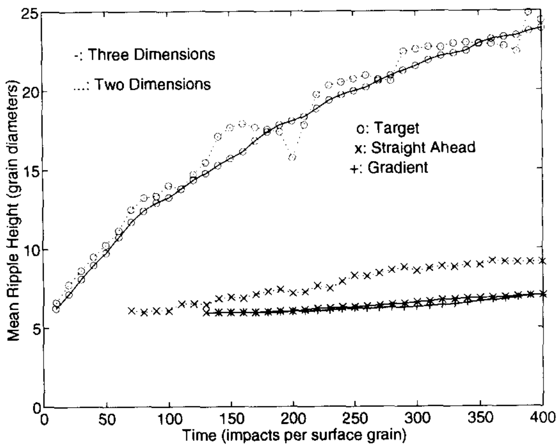

Fig. 10. Mean ripple height vs. time for the target, straight ahead and gradient algorithms in two and three dimensions, illustrating the clear separation in the growth rate of the mean height between the target and the other algorithms.

projected to increase by perhaps as much as 50% at $t = 1200$ (20 min), were it computationally feasible to simulate for that length of time with a larger system. A range of sinuosity and cross-sectional shape can be generated by varying the strength of the components (i.e., target, straight ahead or rolling algorithms) of the reptation transport algorithm. It is clear that the simulation approach outlined here can reproduce the general size, shape and time-evolution characteristics of wind ripples seen in the natural environment.

4.3. *Impact angle*

The effect of the angle to the horizontal with which saltating grains impact the bed on the characteristics of wind ripples will be considered. Although the reptation length varies with impact angle because of the dynamics of the impact (e.g., [18]), it was held fixed to isolate the geometrical influence of the impact angle. Ripple patterns resulting from the target algorithm for impact angles 5°, 10° and 30° are shown in Fig. 11 at $t = 50$. For a 5° impact angle, the region on the downward side of a ripple protected from impacts, the shadow zone [10], is sufficiently

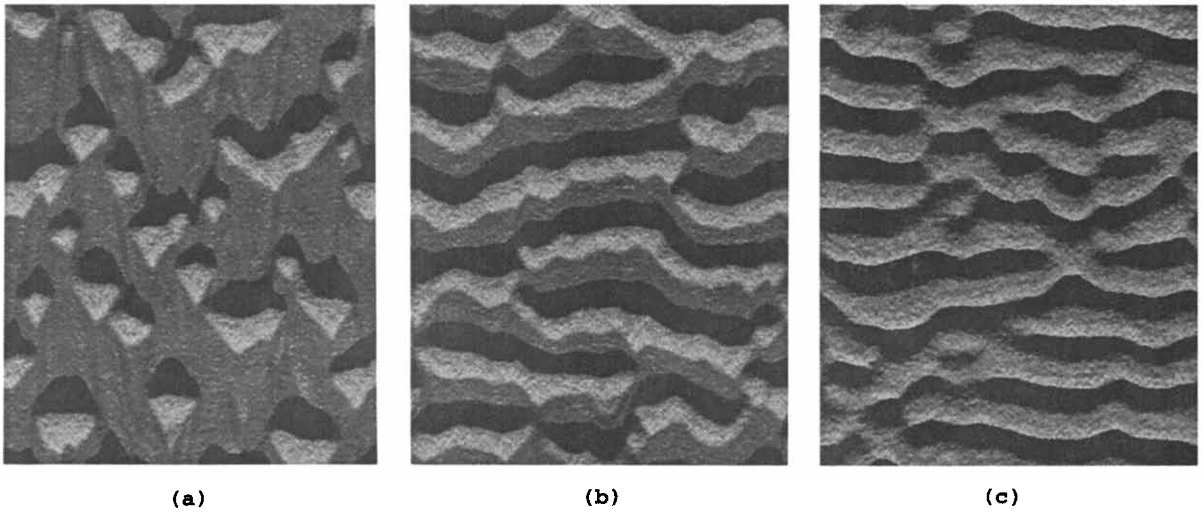

Fig. 11. Plan view of simulated ripples (using the target algorithm) illustrating the effect of varying the saltating grain impact angle. Lighted from the bottom with angle 16° relative to the horizontal. 512×512 periodic lattice ($512d \times 418d$). (a) Impact angle = 5°, (b) 10°, (c) 30°.

long that it inhibits the connection of sand ridges in the cross-wind direction. Between the disconnected ripples is a flat zone at an elevation where the shadow zone of one ripple meets the upwind slope of the next ripple downwind. These inter-ripple flats may correspond to the flat platforms of sand in nature across which ripples sometimes are observed to propagate [10] or to the hollows of ridge and hollow couplets or to interdune flats seen in large dune fields (e.g. [34]). At 10°, the ripples become well-connected, but the flats still exist. At 30°, the shadow zone and flats disappear; however, ripples continue to form in the absence of a shadow zone. If the effect of changing the impact angle is to increase the ripple spacing by changing the length of the shadow zone only, then the ripple index should vary linearly with the inverse of the tangent of the impact angle. An approximate linear dependence is observed for impact angles less than 30°, as shown in Fig. 12.

4.4. Reptation length

The physical parameters in the simulations that can determine the ripple scale are the grain diameter and the reptation length (ignoring the artificial influence of the system size). The variation of mean spacing and height with reptation length at $t = 20$ and $t = 150$ is shown in Figs. 13, 14 for ripples generated with the target algo-

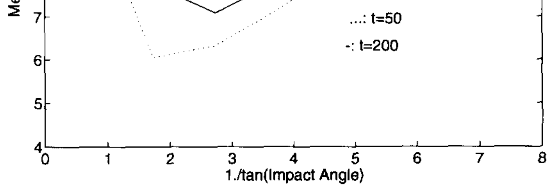

Fig. 12. Mean ripple index vs. inverse of the tangent of the impact angle for target algorithm at two times. If the impact angle is predominantly a geometrical effect (increasing the spacing at a particular height with decreasing impact angle), then the graph should be a straight line. The data are in agreement with this hypothesis for impact angles less than 30°, where salatating grains begin to strike the surface in the downwind "shadow zone" of the ripple.

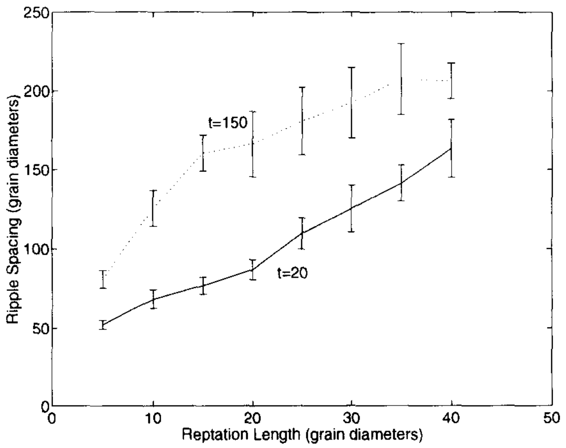

Fig. 13. Mean ripple spacing vs. reptation length for the target algorithm, showing that the spacing roughly scales with reptation length shortly after the ripples are initiated, and that this approximate linear relationship breaks down as the ripples develop. Uncertainties in this and subsequent plots are calculated from the standard deviation of the measured distribution.

rithm. At $t = 20$, in the range $l_r = 5$–$40d$, the spacing varies linearly with l_r, but the height shows no significant dependence on reptation length. At $t = 150$, when the ripples are well-developed, neither spacing nor height vary linearly with reptation length. Rather, the spacing and height increase at a decreasing rate with l_r, much like their dependence on time. These results for reptation length are robust in the sense that they have been observed with other transport algorithms and in two dimensional simulations [23]. The spacing and height do not depend significantly on the downwind or crosswind standard deviation of reptation length.

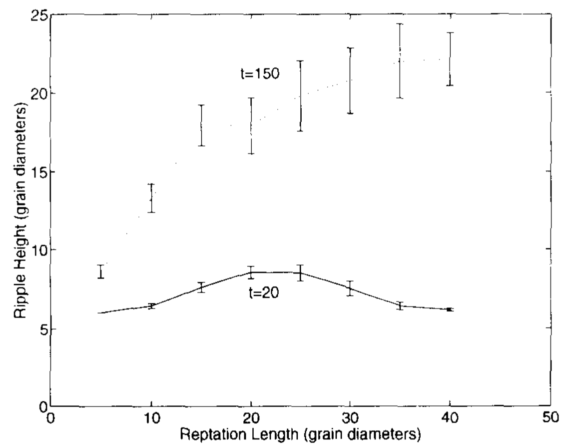

Fig. 14. Mean ripple height vs. reptation length for the target algorithm. The mean height shows no trend shortly after ripple initiation, indicating that ripples originate at a height that is independent of reptation length. After the ripples evolve, the ripple index is approximately independent of reptation length. The conclusion that the scale of ripples is not determined by the reptation length follows from Figs. 13, 14.

The lack of a linear relationship between reptation length and ripple height or spacing leads us to conclude that the scale of ripples varies linearly only with the grain diameter. In other words, the dimensional spatial scale of simulated wind ripples is set by the grain diameter. This trend has been observed clearly in field data [10]. In nature, other parameters, such as impact angle and reptation length, can be functions of the grain diameter, which may obfuscate the strict linear dependence inferred from the simulations.

4.5. Initiation from topography

Saltating grain impacts onto a flat grain bed result in small bumps and depressions owing to the stochastic nature of the impacts. Additional impacts tend to fill in the depressions (because reptating grains are deposited preferentially in depressions) and to remove the bumps (because impacts occur preferentially on bumps). However, this tendency is opposed by the preferential deposition of reptating grains on the upwind slope of bumps, a positive feedback of relief on grain deposition. If the rate of growth by positive feedback exceeds the rate at which bumps and depressions are eliminated, then the bump and depression relief increases, and ripple crests and troughs can develop. The sign of the net growth rate of relief depends on the reptation transport algorithm.

Once a bump becomes large enough to retain reptating grains from its slopes in a downwind shadow zone shielded from impacts, it begins to propagate as a ripple by eroding grains from its upwind slope and depositing them on its downwind slope. Cross-wind organization of the ripple pattern occurs through cross-wind transport resulting from reptation, rolling or settling of grains.

Insight into how ripples become organized in the downwind direction can be gained from studying the development of ripples triggered from existing relief. Two examples are shown in Fig. 15. An initial sand ridge $10d$ in height and $100d$ in the cross-wind direction, with angle of repose slopes, Fig. 15a, gives rise to a series of roughly evenly-spaced troughs and ridges, Figs. 15b,c. A flat region protected from impacts lies downwind of the initial ridge. Just after this shadow zone the surface is depleted of grains by impacts but receives no grains from upwind; therefore, net erosion occurs and a trough develops. The grains excavated from the trough accumulate in a second ridge just downwind of the trough. This sequence can be repeated many times. Incipient ripples formed on other parts of the sand surface are influenced by the presence of the larger ridges, Fig. 15c. A similar pattern develops from an initial trough on a flat surface, Fig. 15d. These patterns are reminiscent of ripples formed from an incipient sand bump in uni-directional underwater flow [35], except that lateral spreading of the pattern, observed for the underwater ripples, is absent in wind ripple simulations. The simulations illustrate the strong interactions between ripples, which evidently can regulate and organize the patterns as it develops.

4.6. *Origin of ripple spacing*

Field observations indicate that the spacing of ripples increases with time at a decreasing rate [3,10,20,29]. This decreasing rate of increase has been interpreted as the approach to a steady-state asymptote. A similar trend is observed with the spacing and the height of simulated ripples, shown in Figs. 16a,b. The asymptotic increase in mean ripple height appears to be compatible with either a logarithmic or a linear dependence on time, as seen in Figs. 16b,c for $t = 300$–600; however, longer-term two-dimensional simulations do not support a linear dependence of height on time [23]. There is no indication that the mean value of height or spacing of simulated ripples will achieve a steady-state value. As was argued above, the only physical length scale to which the spacing and height of well-developed simulated ripples is proportional is the grain diameter.

These observations from the field and from simulations can be explained and reconciled by a theoretical model [3]. The model predicts the time evolution of the mean ripple height by considering ripple interactions resulting in merger or repulsion (Fig. 3). Two theoretical observations form the basis for this model: (i) When a merger occurs, the depth of the trough between the crests of two ripples vanishes, suggesting that ripple height is the key variable, rather than the ripple spacing. (ii) The influence of statistical fluctuations in reptation transport on ripple dynamics are greater when the ripples are small and mergers are common, suggesting a possible link between the occurrence of mergers and the importance of transport fluctuations to the propagation and evolution of a ripple. In the model, the height of a ripple changes only in discrete amounts roughly corresponding to a grain diameter. On the average, the model ripples interact through exchange of grains so as to minimize the size difference of the ripples and therefore their relative propagation speeds. These repulsive interactions would prevail in a continuum model of ripple motion, where transport occurs in infinitesimal packets with no fluctuations. However, the model predicts that statistical fluctuations in the reptation transport flux originating with fluctuations in the saltation impact flux can lead to mergers between ripples and the consequent increase in mean ripple height and spacing, preferentially when the overall size of the interacting ripples is small and the sensitivity to fluctuations is greatest. In sum-

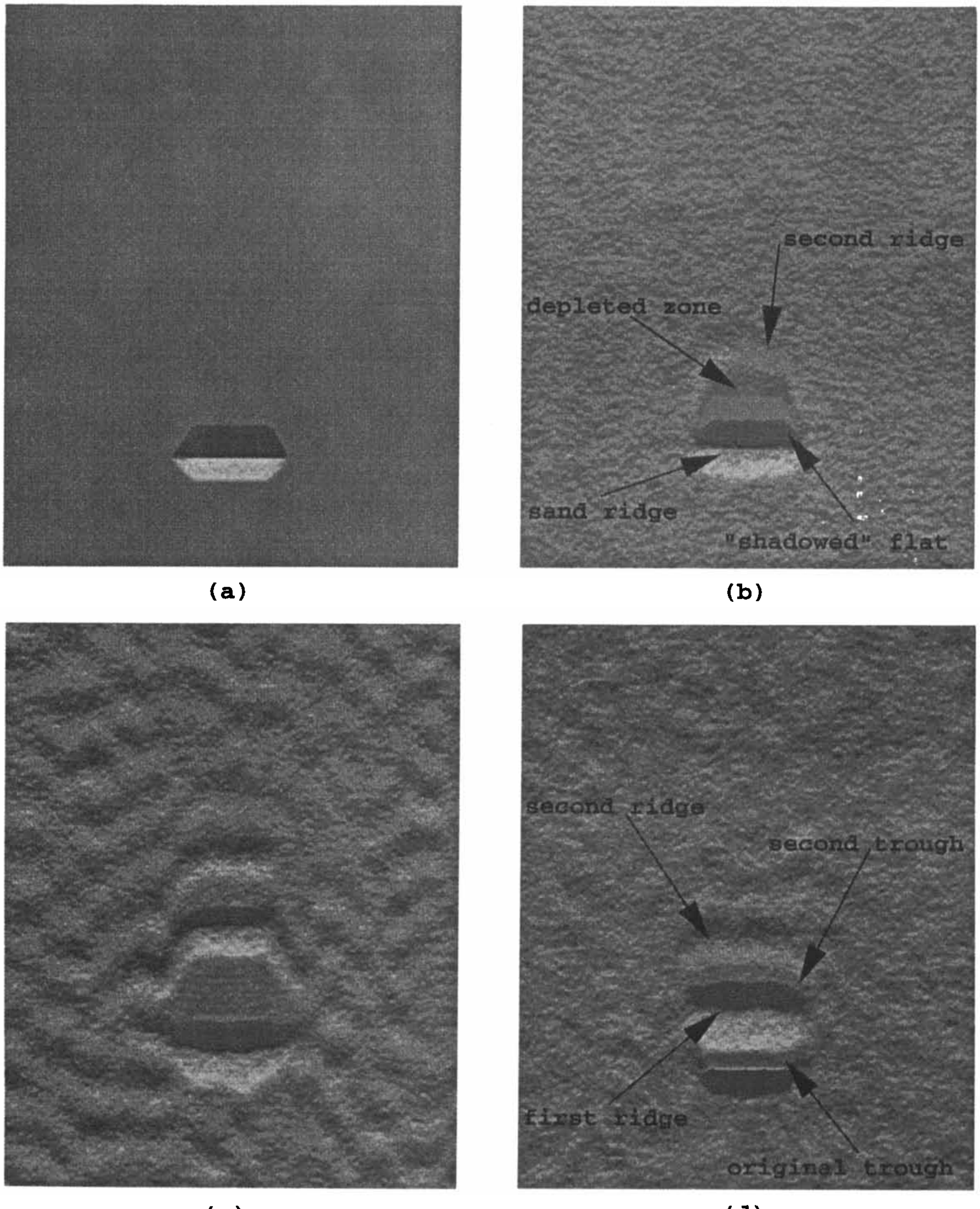

Fig. 15. Plan view of simulated ripple initiation from a ridge and a trough, using the target algorithm. On a 512×512 lattice lighted as in Fig. 6 (a) $t = 0$. Initial ridge ($10d$ high, $100d$ wide with angle-of-repose slopes). (b) $t = 2$. One ridge has developed downwind, separated from the original ridge by a flat region shadowed from impacts. (c) $t = 6$. Three ridges have formed downwind of the original ridge. Note the lateral linking between these ridges and ripples developing from the flat surface. (d) $t = 4$. Two to three troughs have formed downwind of a trough excavated into an initially flat surface.

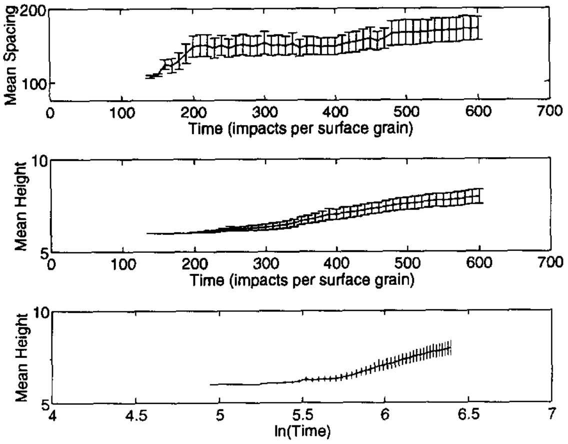

Fig. 16. Plots of mean spacing and height vs. time and mean height vs. logarithm of time for the gradient algorithm. Both spacing and height increase with time. The increase in mean height is consistent with either linear or logarithmic growth.

mary, this negative feedback produces a nearly stable field of ripples of mean size large enough to be relatively immune to the effects of transport fluctuations. The process by which the mean spacing increases by mergers attributable to statistical fluctuations of a finite size was termed *stochastic merging* [3].

A simple, one-dimensional Markov Process formulation of the stochastic merging model predicts that the mean ripple height (and mean wavelength, for constant ripple index) increases logarithmically with time, and that ripple height is proportional to the grain diameter [3]. The former prediction is in accord with the observed increase and apparent stabilization of natural wind ripple spacing because logarithmic growth mimics locally the approach to an asymptote [3]; the latter prediction agrees qualitatively with field observations [10]. Scale separation between the height of a ripple and the grain diameter does not occur in the stochastic merging model. Because of the relationship between mergers and transport fluctuations of finite size, a significant conclusion of the model is that the evolution of wind ripples with time through merger cannot be treated by continuum methods.

The mechanism by which mergers occur and mean ripple size increases in three-dimensional simulations is somewhat more complicated than that pictured in Fig. 3. In the initial phase of ripple development, as the incipient ripples grow and join laterally, many mismatches between ripple crests arise. We term the right-facing ends of ripple crests as viewed while facing downwind (following [36]) terminations and the left-facing ends anti-terminations, Fig. 17a. Terminations and anti-terminations propagate relative to the field of ripples in the downwind direction and they move laterally in the direction that reduces the length of the ripple crest (to the left for terminations, to the right for anti-terminations), as illustrated in the sequence in Figs. 17a–d. A termination attaches to the crest immediately downwind of it, forming a Y-junction, Fig. 17a. Then the downwind fork of the Y breaks off, forming another termination that translates and attaches to the next ripple crest downwind, Figs. 17b–d. In the simulations, terminations and anti-terminations propagate downwind at a speed 2–3 times the mean propagation speed of the ripples, and they translate normal to the wind direction at a speed 1/4 to 1/2 of the mean ripple propagation speed. We emphasize that the behavior of terminations and anti-terminations is the same, except for opposite directions of lateral motion. Termination propagation has been reported for natural wind ripples [36].

As argued by Anderson and McDonald [36], termination propagation through a ripple pattern can be explained by the decrease in height of the ripple with proximity to the termination of its crest. As shown in Fig. 18, the depth of the trough downwind of a ripple crest near a termination, h_B, is less than the height of the ripple far from a termination, h_A. The inverse dependence of ripple propagation speed on h implies that the ripple crest at BB*, close to the termination, propagates faster than the crest at AA*. The lateral translations of terminations can be understood in terms of the stochastic merging model. The small height of the ripple near the

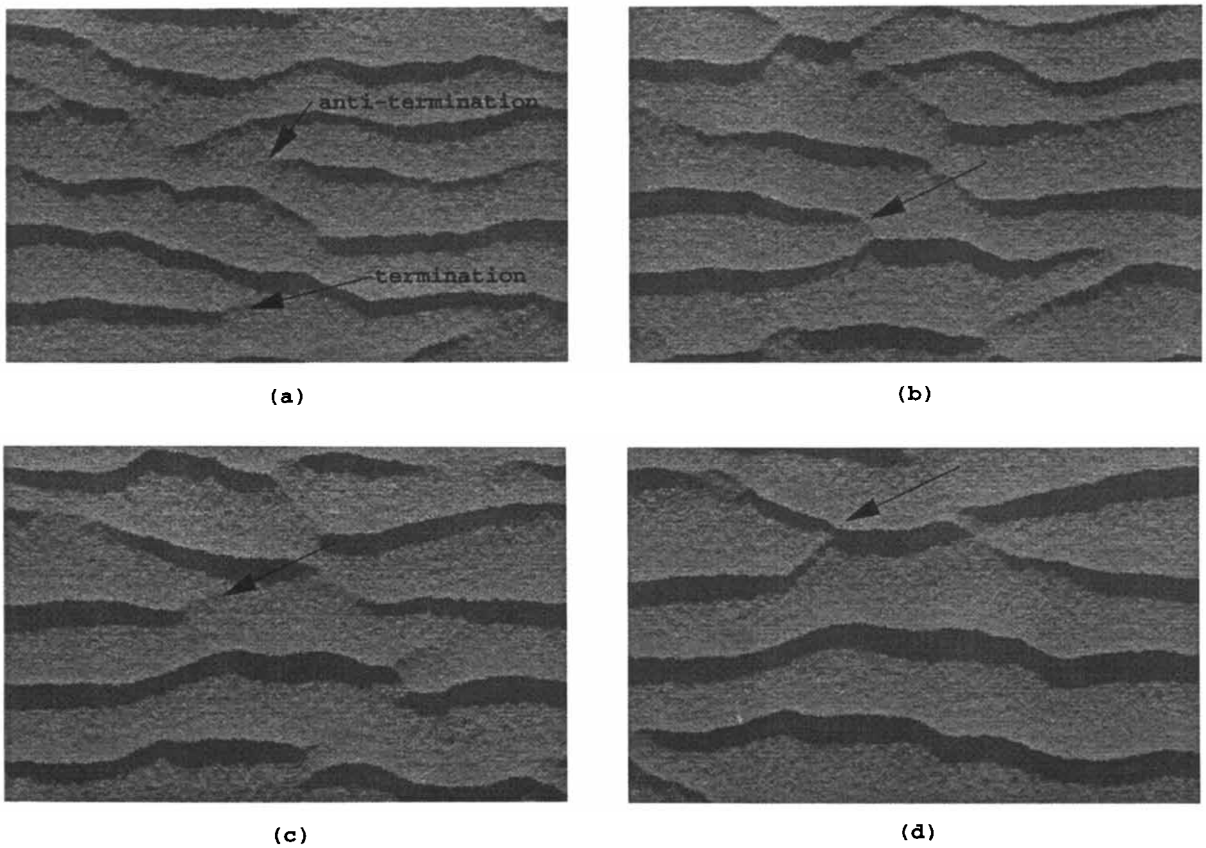

Fig. 17. Plan view of a termination propagating through a field of simulated ripples and to the left. (a) $t = 200$. (b) $t = 250$. (c) $t = 290$. (d) $t = 330$. Lighted as in Fig. 6. Width of field of view = $418d$.

termination enhances the sensitivity to fluctuations and hence increases the probability for merger in that region of the ripple crest. Therefore, at a Y-junction, merger of a portion of the ripple crest near a termination with the ripple immediately downwind shortens the ripple crest that detaches from the Y-junction, as is observed in the simulations, Fig. 17. This decrease in the length of the ripple crest implies an increase in the mean ripple spacing; because, the mean spacing can be expressed as $\lambda = A/L$, where L is the total length of ripple crests in the simulation and A is the (fixed) product of the length and width of the simulation domain. The "quality" of the pattern increases when a leftward travelling ripple crest termination meets and annihilates with a rightward travelling anti-termination, as depicted in Fig. 19.

In the picture of ripple formation presented thus far, the wind ripple pattern initially develops with terminations and anti-terminations that propagate downwind and translate crosswind though the pattern, causing an increase in the mean spacing and a reduction in the number of termination, anti-termination pairs through annihilation. Under this sequence of events, increase in the mean ripple size would cease after all termination pairs had been annihilated. However, in the simulations, one additional ripple behavior complicates this picture. As illustrated in Fig. 20, a termination, anti-termination pair can be created in a field of ripples

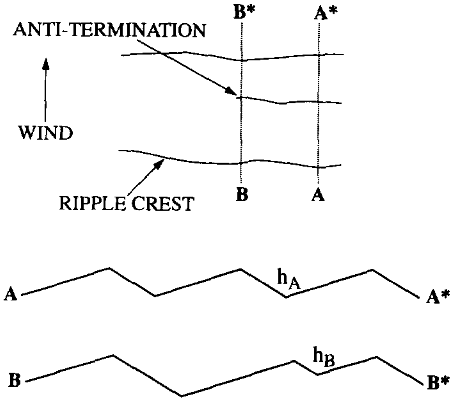

Fig. 18. Interpretation of why terminations and anti-terminations propagate faster than ripples and in the direction that decreases the length of the ripple crest. Top sketch illustrates an anti-termination in plan view. Bottom sketch illustrates the cross sections AA* and BB*. Near a termination, a ripple has a smaller cross-sectional size, suggesting that it propagates faster and is more susceptible to mergers [7].

without pairs. Where one ripple crest approaches another, the two crests can merge at a point, causing a break in the downwind ripple crest, and the consequent creation of a termination/anti-termination pair. This behavior is observed more commonly when the mean ripple spacing is small (e.g., in Fig. 20, $\lambda \sim 51d$). This point is underscored by a comparison of two simulations that started with evenly spaced ripples of two different sizes: $\lambda \sim 51d$, $h = 4$ (Fig. 21a) and $\lambda \sim 102d$, $h = 8$ (Fig. 21c). At $t = 30$ for the smaller ripples, numerous termination pairs have been created, Fig. 21b. By contrast, at $t = 400$ the larger ripples are somewhat less regularly spaced but no termination pairs exist and the mean spacing has not changed, Fig. 21d. The observed dependence of pair creation on ripple size can be interpreted as resulting from the decreasing importance of transport fluctuations with increasing ripple size, following the stochastic merging model. Pair creation in the simulations cannot be reconciled with ripple models that hypothesize that ripple stability results from the winnowing out of ripples of different sizes by mergers [20,37].

5. Discussion

The wind ripple algorithms described in this paper incorporate simple representations of physical processes known to occur in the transport of sand by wind, including transport of surface grains in reptation through randomly placed saltating grain-bed impacts, dependence of reptation length and direction on surface gradient, and the influence of surface gradient and grain inertia on the deposition of reptating grains. The algorithms do not include entrainment of surface grains through direct aerodynamical forces, modification of reptating grain trajectories by the wind, a spatial correlation between saltating grain-bed impacts (i.e., a characteristic hop length for saltating grains), the dynamical interference between two grain-bed impacts that are closely located in space and time, nor the dynamical and geometrical effects resulting from a wide or bimodal distribution of grain sizes. Application of these algorithms to initially flat sand beds leads to topographic patterns for which the spacing, height, cross-sectional shape, plan view pattern and crest termination behavior all fall within the range observed in natural wind ripples. The height and spacing of wind ripples is predicted to scale with grain diameter, in accord with the trend of observations. The simulations results are compatible with the stochastic merging model of wind ripple dynamics [3]. Potential implications of this work are that wind ripples are self-organized and that their form and spacing are not controlled by direct aerodynamical forces on surface grains. In addition, to the extent that the simulations reflect nature and are described by the stochastic merging model, wind ripple time evolution cannot be modeled with spatial continuum methods. Beyond possible application of the insight gained from the simulations to other transverse bedforms, it appears that the scale of at least one additional surficial pattern, sorted stripes, potentially is related to the stochastic merging mechanism [4,40].

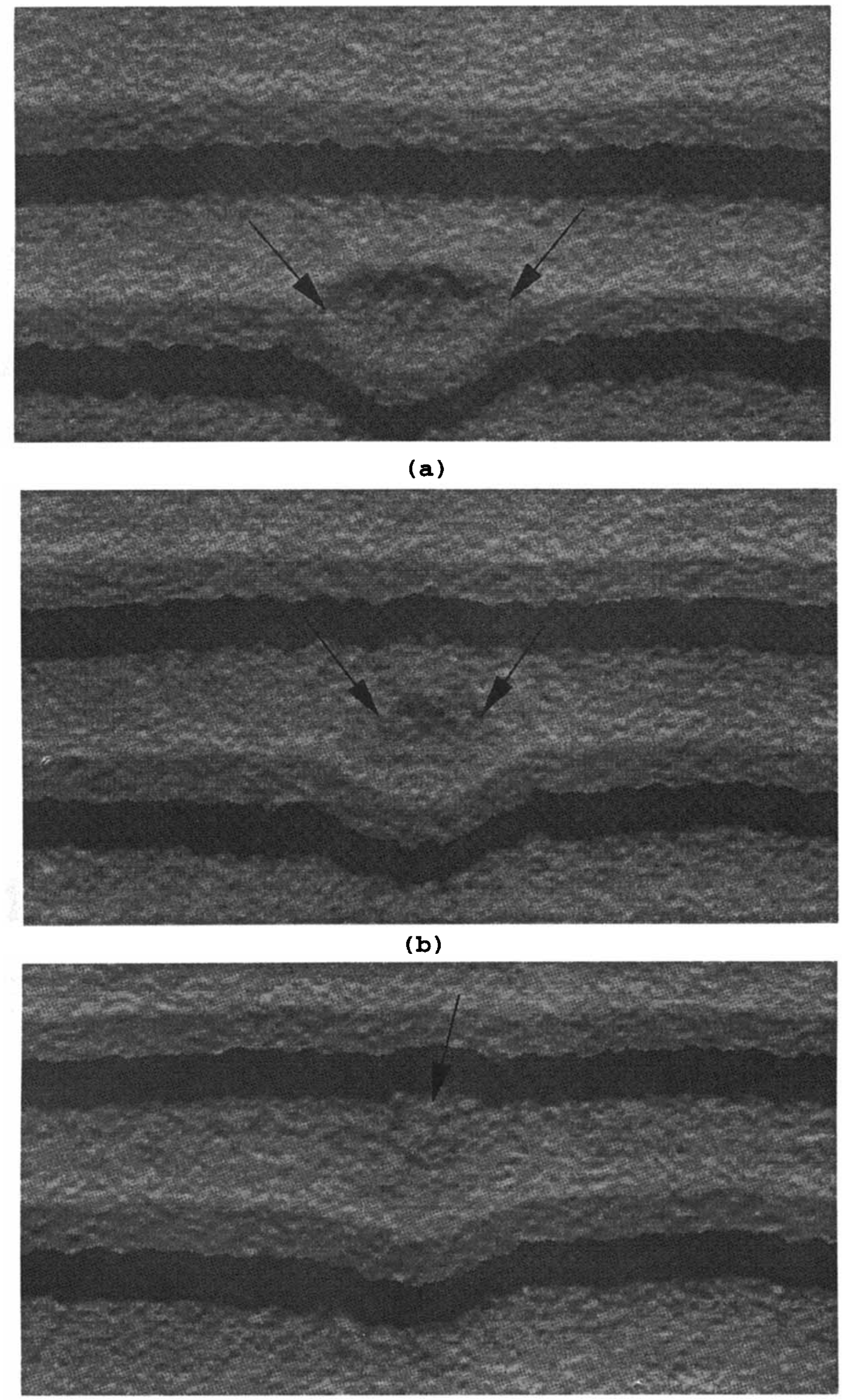

(a)

(b)

(c)

Fig. 19. Plan view of ripples simulated with the gradient algorithm, lighted as in Fig. 6, showing termination/anti-termination annihilation. Width at field of view = $418d$. Time interval between frames is $\Delta t = 10$.

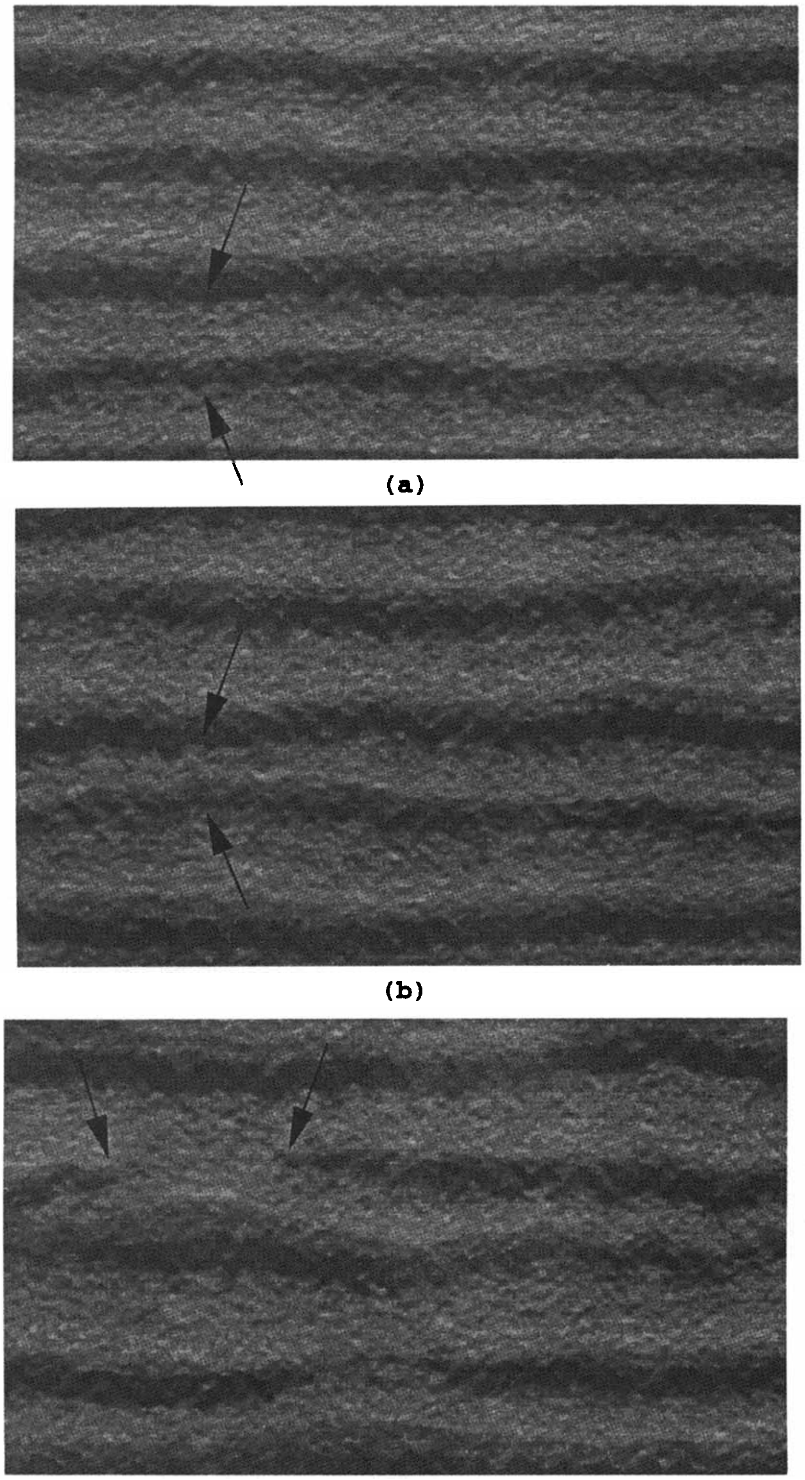

(a)

(b)

(c)

Fig. 20. Plan view of ripples simulated with the gradient algorithm, lighted as in Fig. 6, showing creation of a termination/anti-termination pair. Width of field of view $= 418d$. Time interval between frames is $\Delta t = 10$.

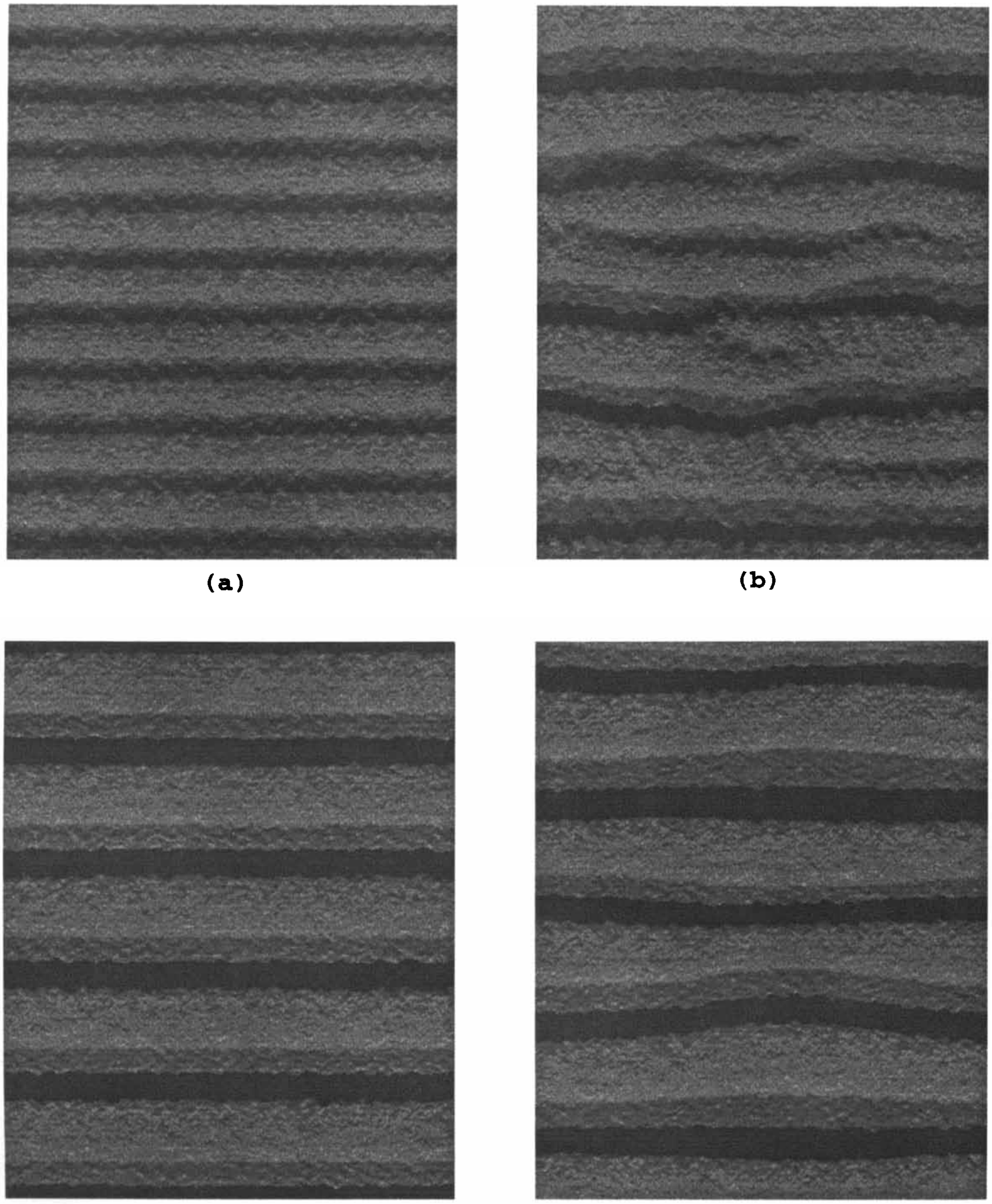

(a) (b) (c) (d)

Fig. 21. Plan view of ripples simulated with the gradient algorithm, lighted as in Fig. 6, comparing the time development of evenly-spaced ripples with mean spacing $51d$, (a), (b) with $\Delta t = 30$, and mean spacing $102d$, (c), (d) with $\Delta t = 380$. The smaller ripples experience pair creation, termination propagation and the consequent increase in spacing, whereas the larger ripples maintain their original mean spacing.

Several improvements to the wind ripple simulations will permit more definite conclusions to be drawn regarding the fundamental nature of wind ripples and other similar bedforms. First, simulations run for a greater length of time and with a larger number of surface grains will facilitate comparisons with theoretical models and with field data. The largest simulations reported here, on 1024×1024 lattices, correspond to a size of only about $25\,\mathrm{cm} \times 21\,\mathrm{cm}$ for dune sand. Some preliminary simulations on 2048×2048 lattices and planned simulations for larger systems will give more accurate results and allow us to detect any subtle dependences of ripple behavior on the size of the system. Second, the geometrical influences on saltating grain-bed impacts, including the effects of surface slope, grain size distribution and sorting, are not well understood. Dynamical simulations of ripple formation, where the motion of the grains is calculated explicitly from interparticle contact and gravitational forces, are beginning to provide insight into the importance of bed geometry in ripple formation [38], although the limitations on system size due to finite computational resources are severe. Finally, the use of more realistic rules for the distribution of surface grains ejected in an impact will allow quantitative comparisons with field data (in contrast to studying the basic physics of wind ripple formation). Toward that end, a distribution of ejected grains based on dynamical computer simulations was utilized in recent two-dimensional simulations of ripple formation [28].

The feedbacks operating in the wind ripple simulations to initiate relief from a flat surface and to organize that relief into regular patterns also have been observed in simulations of other superficial patterns, including wind-blown sand dunes [41]. A variety of positive feedbacks resulting from local transport rules can lead to the initiation of transverse bedforms. For example, transport rules that reduce the transport flux with increasing upstream-facing slope or that increase the flux with increasing elevation robustly result in the development of realistic appearing bedforms. Negative feedbacks operate to stabilize the pattern and to enhance uniformity of spacing or size of the bedforms. For example, the exchange of sediment between transverse bedforms resulting from an inverse dependence of bedform propagation speed on bedform size can act to reduce differences in spacing using a wide variety of transport algorithms. The patterns are insensitive to the detailed character of both positive and negative feedback.

Computer simulations of the type described here have proven useful in elucidating the fundamental physical mechanisms of a number of surficial patterns in geomorphology (e.g., [6,7,28]). By permitting control of the microscopic physics, computer simulations of systems displaying complex behavior offer possibilities for further understanding of the basic physics operating in these systems and of the consequences of particular microscopic rules. In addition, study of natural systems can lead to the discovery of unknown behaviors of complex systems; stochastic merging may be one such behavior.

At present, computer simulations of surficial pattern formation are performed in a mode in which the investigator alters the rules governing the behavior of the system constituents in accordance with feedback from simulation results, constraints from the natural system and physical intuition. However, where it is possible to discretize the constituents of the pattern and the agents of transport, then these rules will be members of a finite, although perhaps large, set. The large number of possible rules may be amenable to classification according to general behavior and effect, as is, for example, the set of rules describing the iterative evolution of one-dimensional cellular automata [39]. The problem of finding the class of microscopic rules that can generate a pattern then can be reduced to a tractable inverse problem, where the pattern is inverted to give the microscopic rules.

Acknowledgments

The authors are grateful to P.K. Haff and T.A. Tombrello for facilitating this collaboration, to P.K. Haff and R.P. Sharp for helpful comments on the manuscript, and to the office of Naval Research, Coastal Sciences and Young Investigators Programs [N00014-92-J-1446], the National Science Foundation, Surficial Processes [EAR-89-15983], and the Division of Physics, Mathematics and Astronomy, California Institute of Technology for support.

References

[1] R. Cooke, A. Warren and A. Goudie, Desert Geomorphology (UCL Press, London, 1993).
[2] G. Willgoose, R.L. Bras and I. Rodriguez-Iturbe, Wat. Res. Res. 27 (1991) 1671.
[3] B.T. Werner and D.T. Gillespie, Phys. Rev. Lett. 71 (1993) 3230.
[4] R.W. Hockney and J.W. Eastwood, Computer Simulation Using Particles (McGraw-Hill, New York, 1981).
[5] U. Frisch, D. d'Humieres, B. Hasslacher, P. Lallemand, Y. Pomeau and J-P. Rivet, Complex Systems 1 (1987) 649.
[6] B.T. Werner and B. Hallet, Nature 361 (1993) 142.
[7] B.T. Werner and T.M. Fink, Science 260 (1993) 968.
[8] W.B. Langbein and L.B. Leopold, USGS Prof. Paper 422-L (1968).
[9] R.A. Bagnold, The Physics of Blown Sand and Desert Dunes (Chapman and Hall, London, 1956).
[10] R.P. Sharp, J. Geology 71 (1963) 617.
[11] V. Cornish, Ocean Waves and Kindred Geophysical Phenomena (Cambridge Univ. Press, Cambridge, 1934).
[12] B.T. Werner, J. Geology 98 (1990) 1.
[13] B.T. Werner and P.K. Haff, Sedimentology 35 (1988) 189.
[14] P.K. Haff and R.S. Anderson, Sedimentology 40 (1993) 175.
[15] I.K. McEwan, B.B. Willetts and M.A. Rice, Sedimentology 39 (1992) 971.
[16] J.E. Ungar and P.K. Haff, Sedimentology 40 (1987) 289.
[17] S. Mitha, M.Q. Tran, B.T. Werner and P.K. Haff, Acta Mech. 63 (1986) 267.
[18] B.T. Werner, Ph.D. Thesis, California Institute of Technology, Pasadena (1987).
[19] B.T. Werner and P.K. Haff, in: Advances in Aerodynamics, Fluid Mechanics and Hydraulics, eds. R.E.A. Arndt, H.G. Stefan, C. Ferrell and S.M. Peterson (American Society of Civil Engineers, New York, 1986) p. 337.
[20] R.S. Anderson, Earth. Sci. Rev. 29 (1990) 77.
[21] R.S. Anderson and P.K. Haff, Science 241 (1990) 820.
[22] B.B. Willetts and M.A. Rice, in: Aeolian Geomorphology, ed. W.G. Nickling (Allen and Unwin, 1986) p. 1.
[23] B.T. Werner, Sedimentology (1993), submitted.
[24] H. Nishimori and N. Ouchi, Phys. Rev. Lett. 71 (1993) 197.
[25] J.F. Kennedy, J. Geophys. Res. 69 (1964) 1517.
[26] R.S. Anderson, Sedimentology 34 (1987) 943.
[27] M. Seppala and K. Linde, Geogr. Annlr. 60 (1978) 29.
[28] S.B. Forrest and P.K. Haff, Science 255 (1992) 1240.
[29] B.T. Werner, in: Patterns in Fluid Flow, Proc. 1991 Summer Study Program in Geophysical Fluid Dynamics (Woods Hole Oceanographic Institution, Woods Hole, MA, 1991) p. 167.
[30] A. von Burkalow, Geol. Soc. Am. Bull. 56 (1945) 669.
[31] B.B. Willetts and M.A. Rice, Earth Surf. Proc. Land. 14 (1989) 719.
[32] B.T. Werner, P.K. Haff, R.P. Livi and R.S. Anderson, Geology 14 (1986) 743.
[33] M. Sorensen, in: Proc. Int. Workshop on the Physics of Blown Sand 1, eds. O.E. Barndorff-Nielsen, J.T. Moller, K. Romer Rasmussen and B.B. Willetts (University of Aarhus Press, Aarhus, Denmark, 1985) p. 141.
[34] R.P. Sharp, Geol. Soc. Am. Bull. (1979) 908.
[35] J.B. Southard and J.R. Dingler, Sedimentology 16 (1971) 251.
[36] R.S. Anderson and R.R. McDonald, presented at the AGU Fall Meeting (1991).
[37] A. Fuhrboter, cited in: Loose Boundary Hydraulics, ed. A.J. Raudkivi (Pergamon, Oxford).
[38] E. Gkioulekas, S.A. Hemdon and B.T. Werner, EOS 74, No. 43 (1993) 340.
[39] S. Wolfram, Physica D 10 (1984) 1.
[40] B.T. Werner and B. Hallet, in preparation.
[41] B.T. Werner, in preparation.